

STELLAR POPULATIONS OF LYMAN ALPHA EMITTERS AT $z \sim 6 - 7$: CONSTRAINTS ON THE ESCAPE FRACTION OF IONIZING PHOTONS FROM GALAXY BUILDING BLOCKS[‡]

YOSHIAKI ONO¹, MASAMI OUCHI^{2,3}, KAZUHIRO SHIMASAKU^{1,4}, JAMES DUNLOP^{5,6},
DUNCAN FARRAH^{7,8}, ROSS MCLURE⁶, AND SADANORI OKAMURA^{1,4}

Accepted for publication in ApJ

ABSTRACT

We investigate the stellar populations of Ly α emitters (LAEs) at $z = 5.7$ and 6.6 in a 0.65 deg^2 sky of the Subaru/*XMM-Newton* Deep Survey (SXDS) Field, using deep images taken with Subaru/Suprime-Cam, UKIRT/WFCAM, and Spitzer/IRAC. We produce stacked multiband images at each redshift from 165 ($z = 5.7$) and 91 ($z = 6.6$) IRAC-undetected objects, to derive typical spectral energy distributions (SEDs) of $z \sim 6 - 7$ LAEs for the first time. The stacked LAEs have as blue UV continua as the HST/WFC3 z -dropout galaxies of similar M_{UV} , with a spectral slope $\beta \sim -3$, but at the same time they have red UV-to-optical colors with detection in the $3.6 \mu\text{m}$ band. Using SED fitting we find that the stacked LAEs have low stellar masses of $\sim (3 - 10) \times 10^7 M_{\odot}$, very young ages of $\sim 1 - 3$ Myr, negligible dust extinction, and strong nebular emission from the ionized interstellar medium, although the $z = 6.6$ object is fitted similarly well with high-mass models without nebular emission; inclusion of nebular emission reproduces the red UV-to-optical colors while keeping the UV colors sufficiently blue. We infer that typical LAEs at $z \sim 6 - 7$ are building blocks of galaxies seen at lower redshifts. We find a tentative decrease in the Ly α escape fraction from $z = 5.7$ to 6.6 , which may imply an increase in the intergalactic medium neutral fraction. From the minimum contribution of nebular emission required to fit the observed SEDs, we place an upper limit on the escape fraction of ionizing photons to be $f_{\text{esc}}^{\text{ion}} \sim 0.6$ at $z = 5.7$ and ~ 0.9 at $z = 6.6$. We also compare the stellar populations of our LAEs with that of stacked HST/WFC3 z -dropout galaxies.

Subject headings: cosmology: observations — galaxies: formation — galaxies: evolution — galaxies: high-redshift — galaxies: stellar content —

1. INTRODUCTION

Ly α emitters (LAEs) are a galaxy population commonly seen at high redshift. The high number density of LAEs indicates their importance in the evolutionary history of galaxies. Since galaxies with strong Ly α emission can be identified as LAEs even when their continuum emission is too faint to be detected in broadband imaging, LAEs provide an opportunity to probe low-mass galaxies with active star-formation. Some of them may be building blocks of more evolved galaxies.

Surveys of LAEs have been made primarily with narrow-band imaging to isolate Ly α emission (e.g., Hu et al. 1998; Rhoads et al. 2000; Iye et al. 2006), and until now over a thousand LAEs have been photometrically selected and/or spectroscopically identified (e.g., Hu et al. 2002; Ouchi et al.

2003; Malhotra & Rhoads 2004; Taniguchi et al. 2005; Kashikawa et al. 2006; Shimasaku et al. 2006; Dawson et al. 2007; Gronwall et al. 2007; Murayama et al. 2007; Ouchi et al. 2008; Shioya et al. 2009; Nilsson et al. 2009; Guaita et al. 2010; Hayes et al. 2010).

Studying the stellar population of LAEs is essential to understand their physical nature and to reveal the relationship between LAEs and other high-redshift galaxies such as Lyman break galaxies (e.g., Steidel et al. 1996). At $z \simeq 3 - 5$, much progress has been made recently, and it has been revealed from large samples with multiband photometry that most LAEs are small galaxies with masses $10^8 - 10^9 M_{\odot}$ and young ages $< 10^8$ yr (e.g., Gawiser et al. 2007; Nilsson et al. 2007; Pirzkal et al. 2007), while some have large stellar masses of $\simeq 10^{10} M_{\odot}$ (e.g., Lai et al. 2008; Finkelstein et al. 2009; Ono et al. 2010).

At higher redshifts, a few studies have reported on stellar populations of LAEs, but they are all based on a very small sample and consensus has not been reached. Lai et al. (2007) have studied stellar populations of three bright LAEs at $z = 5.7$ detected in rest-frame optical wavelengths, and found that they have high stellar masses of $\sim 10^{10} M_{\odot}$, as old ages as the Universe at their redshifts, and some amount of dust. Ouchi et al. (2009a) have reported the discovery of a giant LAE at $z = 6.595$, Himiko, with a Spitzer/Infrared Array Camera (IRAC; Fazio et al. 2004) counterpart, and estimated its stellar mass to be $(0.9 - 5.0) \times 10^{10} M_{\odot}$. It should be noted that these four LAEs are all detected in at least one IRAC

ono_at_astron.s.u-tokyo.ac.jp

¹ Department of Astronomy, Graduate School of Science, The University of Tokyo, Tokyo 113-0033, Japan

² Observatories of the Carnegie Institution of Washington, 813 Santa Barbara Street, Pasadena, CA 91101, USA

³ Carnegie Fellow

⁴ Research Center for the Early Universe, Graduate School of Science, The University of Tokyo, Tokyo 113-0033, Japan

⁵ Department of Physics and Astronomy, University of British Columbia, 6224 Agricultural Road, Vancouver V6T 1Z1, Canada

⁶ SUPA Institute for Astronomy, University of Edinburgh, Royal Observatory, Edinburgh EH9 3HJ, UK

⁷ Department of Astronomy, Cornell University, Ithaca, NY 14853

⁸ Astronomy Centre, University of Sussex, Falmer, Brighton, UK

[‡] Based on data collected at the Subaru Telescope, which is operated by the National Astronomical Observatory of Japan.

band, which means that they are not typical LAEs but rare, massive-end objects among the overall LAE population. On the other hand, Pirzkal et al. (2007) have studied three faint LAEs at $5.2 \leq z \leq 5.8$ found by Hubble Space Telescope (HST)/Advanced Camera for Survey (ACS) slitless spectroscopy in the Hubble Ultra Deep Field (HUDF), to show that they are all very young (\simeq several $\times 10^6$ yr) with low masses ($\simeq 10^6 - 10^8 M_\odot$) and small dust extinctions ($A_V = 0 - 0.1$). Chary et al. (2005) have studied a gravitationally-lensed LAE at $z = 6.56$, HCM6A, and reported that it has a stellar mass of $\sim 10^9 M_\odot$ and very young age (~ 5 Myr). Although these two studies may be picking up typical LAEs at each redshift, it is hard to draw robust conclusions from such small numbers of objects.

Recently, Ouchi et al. (2008) and Ouchi et al. (2009a) have constructed the largest available sample of $z = 5.7$ and 6.6 LAEs in an about 1 deg^2 of the Subaru/*XMM-Newton* Deep Field (SXDF) from deep optical broadband and narrowband data. About 65% of the field is also covered by deep *JHK* images taken with the United Kingdom Infrared Telescope (UKIRT)/ Wide Field Infrared Camera (WFCAM; Casali et al. 2007) from UKIRT Infrared Deep Sky Survey (UKIDSS) Ultra Deep Survey (UDS; Lawrence et al. 2007; Warren et al. 2007), and $3.6 - 8.0 \mu\text{m}$ images taken with the Spitzer/IRAC from the Spitzer legacy survey of the UDS field (SpUDS; Spitzer Proposal ID #40021; PI: J. Dunlop). In this paper we use these wide-field, multiwaveband survey data to study the stellar population of typical LAEs at $z = 5.7$ and 6.6 from stacking a large number of faint objects (165 at $z = 5.7$ and 91 at $z = 6.6$). At each redshift the stacked object is detected in several broadbands including the $3.6 \mu\text{m}$ band, enabling us to place meaningful constraints on stellar population parameters. We also examine the stellar population of z -dropout galaxies recently discovered in the deep HST/Wide Field Camera 3 (WFC3) data of the HUDF, using the stacked spectral energy distribution (SED) obtained by Labbé et al. (2010) from 14 objects of the Oesch et al. (2010) sample.

As noted by Schaerer & de Barros (2009), careful SED fittings including nebular emission are required to accurately determine stellar population parameters for high- z galaxies (see also Zackrisson et al. 2008; Raiter et al. 2010; Schaerer & de Barros 2010). Nebular emission is produced in the interstellar medium (ISM) ionized by hot stars. Hence, the nebular emission of a galaxy increases as the fraction of ionizing photons absorbed by HI gas in the ISM increases, or equivalently, as the fraction of ionizing photons escaping from the galaxy, $f_{\text{esc}}^{\text{ion}}$, decreases. To see the influence of nebular emission on the determination of stellar population parameters, we examine SED models for two extreme $f_{\text{esc}}^{\text{ion}}$ values: $f_{\text{esc}}^{\text{ion}} = 1$ where the SED is determined solely by stellar emission as most previous studies assumed, and $f_{\text{esc}}^{\text{ion}} = 0$ where the contribution of nebular emission to the SED is largest. We find that the latter models generally give a very good fit to the observed SEDs, especially the $z = 5.7$ one which is fit by the latter significantly better.

In addition, we treat $f_{\text{esc}}^{\text{ion}}$ as a free parameter in our SED fitting to place rough constraints on $f_{\text{esc}}^{\text{ion}}$, because redshifts of $z \sim 6 - 7$ are close to the end of cosmic reionization (e.g., Fan et al. 2006; Becker et al. 2007) and the

$f_{\text{esc}}^{\text{ion}}$ of galaxies is a key parameter which determines the ionizing photon budget. At redshifts up to $z \sim 4$, the $f_{\text{esc}}^{\text{ion}}$ of galaxies has been estimated or constrained by a variety of methods using, e.g., FUV spectra and narrow-band images of star-forming galaxies (e.g., Steidel et al. 2001; Shapley et al. 2006; Iwata et al. 2009) and the distribution of neutral hydrogen column densities in the afterglow spectra of long duration GRBs (e.g., Chen et al. 2007; Fynbo et al. 2009), although the results do not agree well with each other. For example, Shapley et al. (2006) have derived $f_{\text{esc}}^{\text{ion}} \geq 0.65$ for two $z \sim 3$ LBGs with detected Lyman continua and $f_{\text{esc}}^{\text{ion}} = 0.14$ from a composite spectrum of 14 $z \sim 3$ LBGs¹⁰, while Chen et al. (2007) have placed an upper limit of $f_{\text{esc}}^{\text{ion}} \leq 0.075$ using a compiled sample of 28 GRBs (see also Fynbo et al. 2009).

At redshifts as high as $z \sim 6 - 7$, most constraints are based on the UV luminosity density of galaxies. For example, Ouchi et al. (2009b) and Finkelstein et al. (2010) inferred the production rate of ionizing photons in galaxies from the observed UV luminosity density of z -dropout galaxies and obtained lower limits to $f_{\text{esc}}^{\text{ion}}$ to keep the intergalactic medium (IGM) ionized. However, this method has a number of uncertainties such as the UV luminosity function of galaxies and the clumpiness of the IGM. Recently, Bouwens et al. (2010b) proposed that the very blue UV color of z -dropout galaxies they found may be due to weak nebular emission and hence high $f_{\text{esc}}^{\text{ion}}$, because strong nebular emission makes the UV color too red. This is interesting in relating the SED to $f_{\text{esc}}^{\text{ion}}$. However, as they already state, $f_{\text{esc}}^{\text{ion}}$ is not uniquely determined from the UV color but it also depends on the age of the stellar population. In this paper we show that inclusion of a UV-to-optical color reduces this degeneracy and provides constraints on $f_{\text{esc}}^{\text{ion}}$ for our LAEs.

The outline of this paper is as follows. After describing the imaging data used in this study in Section 2, we produce stacked images in Section 3. Our SED fitting method is presented in Section 4. In Section 5, we present and discuss our SED fitting results and constraints on $f_{\text{esc}}^{\text{ion}}$. A summary is given in Section 6. Throughout this paper, we use magnitudes in the AB system (Oke & Gunn 1983) and assume a flat universe with $(\Omega_m, \Omega_\Lambda, h) = (0.3, 0.7, 0.7)$. The age of the universe is $\simeq 0.98$ Gyr at $z = 5.70$ and $\simeq 0.82$ Gyr for $z = 6.56$.

2. DATA

Deep *BVRi'z'* images of the SXDF were taken with Suprime-Cam (Miyazaki et al. 2002) on the Subaru Telescope by the Subaru/*XMM-Newton* Deep Survey project (SXDS; Furusawa et al. 2008). Ouchi et al. (2008) and Ouchi et al. (2009a) combined this public data set with their own imaging data taken with Suprime-Cam through two narrowband filters, *NB816* ($\lambda_c = 8150 \text{ \AA}$, FWHM = 120 \AA) and *NB921* ($\lambda_c = 9196 \text{ \AA}$, FWHM = 132 \AA), and constructed samples of 401 $z = 5.7$ and 207 $z = 6.6$ LAEs over a sky area of $\simeq 1 \text{ deg}^2$ by applying the following selection criteria: (i) existence of a narrowband excess, (ii) no detection in any bandpasses

¹⁰ They have assumed the intrinsic UV to Lyman continuum flux density ratio to be 3.0, and corrected for IGM absorption.

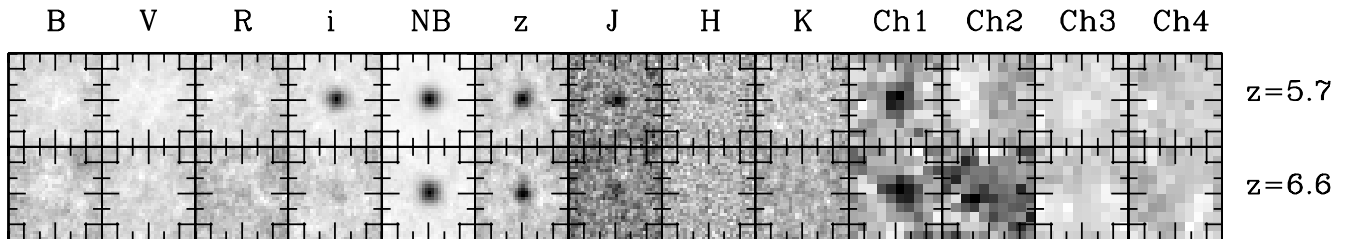


FIG. 1.— Median-stacked images of LAEs at $z = 5.7$ (top) and $z = 6.6$ (bottom) taken by the Subaru Suprime-Cam (B, V, R, i', NB, z'), the UKIRT WFCAM (J, H, K), and the Spitzer IRAC ($3.6\mu\text{m}, 4.5\mu\text{m}, 5.8\mu\text{m}, 8.0\mu\text{m}$). The $z = 5.7$ LAE is detected (brighter than the 3σ magnitude) in $i', NB816, z'$, and $3.6\mu\text{m}$, and nearly detected in J . The $z = 6.6$ LAE is detected in $NB921, z'$, and $3.6\mu\text{m}$. Each panel is $6'' \times 6''$ in size, or $\simeq 35$ (33) kpc at $z = 5.70$ (6.56).

TABLE 1
MEDIAN-STACKED LYMAN ALPHA EMITTERS
AT $z = 5.7$ AND 6.6

	$z = 5.7$ LAE	$z = 6.6$ LAE
NB^a	25.5 (27.6)	25.6 (27.0)
m_{con}^b	27.2 (28.2)	27.4 (26.6)
B	99.9 (30.4)	99.9 (30.1)
V	99.9 (29.8)	99.9 (29.5)
R	99.9 (29.9)	99.9 (29.7)
i'	27.9 (30.0)	29.9 (29.6)
z'	27.5 (29.0)	27.7 (28.6)
J	27.6 (27.5)	27.7 (27.1)
H	99.9 (26.6)	99.9 (26.3)
K	99.9 (27.0)	99.9 (26.7)
$3.6\mu\text{m}$	26.7 (27.0)	26.6 (26.7)
$4.5\mu\text{m}$	32.0 (26.6)	26.7 (26.3)
$5.8\mu\text{m}$	99.9 (25.4)	99.9 (24.4)
$8.0\mu\text{m}$	99.9 (25.3)	99.9 (24.1)
β^c	-2.9 ± 1.0	-3.0 ± 2.7
$f(\text{Ly}\alpha)$ [$10^{-18} \text{erg s}^{-1} \text{cm}^{-2}$] ^d	11.0 ± 0.77	8.93 ± 1.25
$L(\text{Ly}\alpha)$ [$10^{42} \text{erg s}^{-1}$] ^d	3.90 ± 0.27	4.37 ± 0.61
$\text{EW}(\text{Ly}\alpha)_{\text{rest}}$ [\AA] ^d	$78.1^{+96.3}_{-65.4}$	$84.2^{+170.8}_{-49.3}$
redshift ^e	5.70	6.56

NOTE. — All magnitudes are total magnitudes. 99.9 mag means negative flux densities. Magnitudes in parentheses are 3σ limiting magnitudes.

^a $NB816$ for $z = 5.7$ LAE, $NB921$ for $z = 6.6$ LAE.

^b Rest-frame UV continuum magnitudes at (observed) effective wavelengths of 8303\AA ($z = 5.7$) and 9445\AA ($z = 6.6$) after correction for $\text{Ly}\alpha$ emission and the IGM absorption, derived from $NB816$ and i' magnitudes ($z = 5.7$) and $NB921$ and z' magnitudes ($z = 6.6$).

^c Derived from m_{con} and J magnitude using eq. (1)

^d Derived assuming that the redshifted $\text{Ly}\alpha$ line is at the center of the NB filter.

^e Corresponding to the central wavelengths of $NB816$ and $NB921$.

blueward of the Lyman limit, and (iii) existence of a spectral break due to IGM absorption. The $z = 5.7$ LAEs have $L(\text{Ly}\alpha) \gtrsim 3 \times 10^{42} \text{erg s}^{-1}$ and $\text{EW}(\text{Ly}\alpha) \gtrsim 27 \text{\AA}$ (Ouchi et al. 2008), and the $z = 6.6$ LAEs have $L(\text{Ly}\alpha) \gtrsim 3 \times 10^{42} \text{erg s}^{-1}$ and $\text{EW}(\text{Ly}\alpha) \gtrsim 14 \text{\AA}$ (Ouchi et al. 2010).

About 77% of the SXDF Suprime-Cam field was imaged in the $J, H,$ and K bands with the wide-field near infrared camera WFCAM on the UKIRT in the UKIDSS/UDS project (Lawrence et al. 2007). The UKIDSS/UDS is underway, and we use Data Release 5 for this study. We align the J, H, K images with the SXDS optical images using common, bright stars, and then smooth them with Gaussian filters so that the PSF

sizes of the J, H, K images match those of the optical images (FWHM $\approx 1.''0$). The 3σ limiting magnitudes over a $2''$ -diameter aperture are calculated to be 24.5, 24.2, and 24.4 in the J, H, K bands, respectively. Because the zero-point magnitudes for the J, H, K images are given in the Vega system, we convert them into AB magnitudes using the offset values given in Table 7 of Hewett et al. (2006).

The SpUDS covers 0.65deg^2 of the overlapping area of the SXDS and UDS fields. This 0.65deg^2 area corresponds to an effective survey volume of $6.0 \times 10^5 \text{Mpc}^3$ for $z = 5.7$ LAEs and $5.2 \times 10^5 \text{Mpc}^3$ for $z = 6.6$ LAEs, respectively. All of the SpUDS IRAC images are geometrically matched to the optical images. We calculate the 3σ limiting magnitude over a $3''$ -diameter aperture to be 24.8, 24.5, 22.7, and 22.6 in the 3.6, 4.5, 5.8, and $8.0\mu\text{m}$ IR AC bands, respectively.

3. STACKING ANALYSIS

In this paper, we only analyze LAEs in the overlapping area of 0.65deg^2 where the Suprime-Cam, WFCAM, and IRAC data are all available. We perform IRAC Channel 1 photometry with a $3''$ -diameter aperture at the position of LAEs in the narrowband images, using the IRAF task `phot`. Among a total of 189 (106) LAEs at $z = 5.7$ (6.6), 165 (91) are found to be fainter than the IRAC $3.6\mu\text{m}$ -band 3σ magnitude (i.e., 24.8 mag), which means that they are neither rare massive-end objects among the overall LAE population, nor confused by neighboring objects. We make their median-stacked multi-waveband images separately for the two redshifts. Their cutouts are shown in Figure 1.

Among those not used for stacking, some seem to have counterparts in the IRAC $3.6\mu\text{m}$ image. However, they have not been spectroscopically confirmed, except for the giant LAE Himiko already studied by Ouchi et al. (2009a). We will discuss elsewhere stellar populations of these bright LAE candidates after we confirm their redshifts by spectroscopy.

3.1. Photometry

We perform $BVRi'z'JHK$ photometry with a $2''$ -diameter aperture at the position of the LAEs in the narrowband images, using the IRAF task `phot`. We then convert them into total magnitudes by subtracting aperture correction terms¹¹, which are evaluated for bright

¹¹ Aperture correction terms [ABmag] are 0.147(B), 0.115(V), 0.146(R), 0.202(i'), 0.156(z'), 0.196(J), 0.208(H), 0.173(K).

and isolated point sources in each band. To evaluate the aperture correction term for the two narrow bands, we measure fluxes for bright point sources in a series of apertures from $2''$ up to $6''$ with an interval of $0.1''$. Since we find that the fluxes level off for $> 5''$ apertures, we define the difference in magnitude between the $2''$ and $5''$ aperture magnitudes as the aperture correction term. For the Spitzer/IRAC four bands, we measure $3''$ -diameter aperture magnitudes for each LAE and converted them to total magnitudes by applying the aperture correction given by Multiwavelength Survey by Yale-Chile (MUSYC) survey¹². The correction values are 0.52, 0.55, 0.74, and 0.86 mag for $3.6\mu\text{m}$, $4.5\mu\text{m}$, $5.8\mu\text{m}$, and $8.0\mu\text{m}$, respectively. We measure the limiting magnitude for each band by making 1000 median-stacked sky noise images, each of which is made of (165 for $z = 5.7$ and 91 for $z = 6.6$) randomly-selected sky noise images. Table 1 summarizes their photometry, UV spectral slope β (see Section 3.2), average $f(\text{Ly}\alpha)$, $L(\text{Ly}\alpha)$, and $\text{EW}(\text{Ly}\alpha)$. We find that the both stacked objects are brighter than the 3σ magnitude in the $3.6\mu\text{m}$ band.

Since our i' -band photometry for the $z = 5.7$ LAE and z' -band photometry for the $z = 6.6$ LAE are contaminated by $\text{Ly}\alpha$ emission and IGM absorption, we derive the emission-free continuum magnitude m_{con} at $\simeq 8303\text{\AA}$ for $z = 5.7$ and at $\simeq 9445\text{\AA}$ for $z = 6.6$, respectively. We obtain $m_{\text{con}} = 27.22 \pm 0.14$ from NB816 - and i' -band photometry, and $m_{\text{con}} = 27.43 \pm 0.57$ from NB921 - and z' -band photometry, taking account of the contributions of $\text{Ly}\alpha$ emission and IGM absorption (Madau 1995) to the photometry in each bandpass (Shimasaku et al. 2006). We use m_{con} instead of the i' -band (z' -band) magnitude for the $z = 5.7$ ($z = 6.6$) LAE to derive the UV spectral slope β in Section 3.2 and constrain the stellar population in Section 4.

3.2. UV Spectral Slope

We estimate the slope of the rest-frame UV continuum, β , from two broad-band magnitudes, m_1 and m_2 :

$$\beta = -\frac{m_1 - m_2}{2.5 \log(\lambda_c^1 / \lambda_c^2)} - 2. \quad (1)$$

where λ_c^1 and λ_c^2 are the central wavelengths of the two broadbands. For the $z = 5.7$ LAE, we set $(m_1, m_2) = (m_{\text{con}}, m_J)$ and obtain $\beta = -2.9 \pm 1.0$, where m_{con} is the continuum magnitude at 8303\AA (see Table 1) and $\lambda_c^J = 12500\text{\AA}$ (Tokunaga et al. 2002). These wavelengths correspond to rest-frame 1240\AA and 1870\AA , respectively. Similarly, $\beta = -3.0 \pm 2.7$ is obtained for the $z = 6.6$ LAE from the continuum magnitude at 9445\AA and m_J , corresponding to 1250\AA and 1650\AA , respectively. Thus both have a very blue slope, although the uncertainty is large especially for the $z = 6.6$ object.

Figure 2 plots β against the rest-frame UV absolute magnitude, M_{UV} , for our objects together with LAEs at two lower redshifts ($z = 3.1$ and 3.7) and LBGs at $z \sim 4, 6$, and 7 . For the LAEs we calculate β using our own data (Ono et al. 2010): $\beta = -2.6 \pm 0.2$ for $z = 3.1$ and $\beta = -2.0 \pm 0.2$ for $z = 3.7$ from R and z' magnitudes,

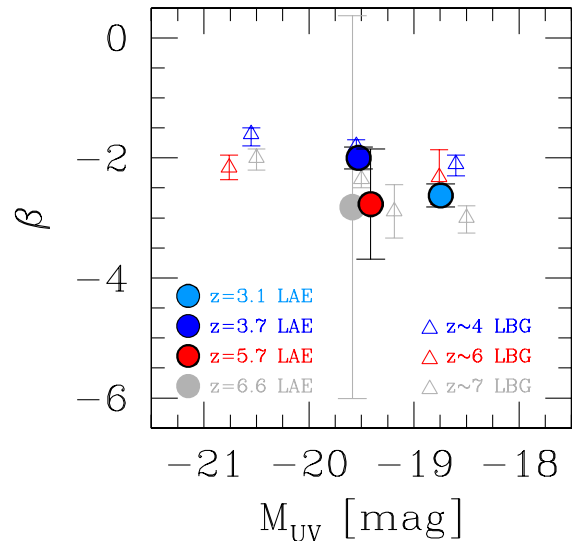


FIG. 2.— UV continuum slope β versus rest-frame UV absolute magnitude M_{UV} . The filled circles and open triangles represent LAEs and LBGs, respectively, colored according to their redshifts. The red and gray circles are our LAEs at $z = 5.7$ and 6.6 , respectively, where the M_{UV} of the $z = 6.6$ LAE has been shifted -0.15 for clarity. Also shown are the values for stacked LAEs at $z = 3.1$ (cyan circle) and $z = 3.7$ (blue circle) (Ono et al. 2010), $z \sim 4$ LBGs (blue triangles: Bouwens et al. 2010b), $z \sim 6$ LBGs (red triangles: Bouwens et al. 2009), and $z \sim 7$ LBGs (gray triangles: Bouwens et al. 2010b; Labbé et al. 2010).

whose rest-frame wavelengths are 1580\AA and 2190\AA for $z = 3.1$ and 1390\AA and 1930\AA for $z = 3.7$. For the LBGs at $z \sim 4, 6$, and 7 , we take the values given in Bouwens et al. (2009, 2010b). In addition, we calculate $\beta = -2.9 \pm 0.4$ for the $z \sim 7$ stacked LBG from its J and H magnitudes¹³ given in Labbé et al. (2010).

We see a weak correlation in the LBGs of individual redshifts that fainter objects have smaller β , i.e., bluer spectra, and a tendency that β at fixed M_{UV} appears to become smaller with redshift. A similar correlation can be seen for the LAEs at $z = 3.1$ and 3.7 if we assume that evolution between these redshifts is negligible and treat them collectively as $z \sim 3.5$ objects. In comparison with this possible correlation seen in LAEs at $z \sim 3.5$, the LAEs at $z = 5.7$ and 6.6 are offset toward smaller β , although the significance is at most 1σ levels due to the large uncertainties in the β measurement especially at $z = 6.6$. This offset, if real, might suggest that the stellar populations of typical LAEs at $z \sim 6 - 7$ are younger, more metal-poor, and/or with less dust than those at $z \sim 3.5$.

Moreover, the LAEs at $z = 5.7$ and 6.6 are slightly below the $\beta - M_{\text{UV}}$ correlation of $z \sim 6$ and 7 LBGs. Although the difference between LAEs and LBGs at $z \sim 6 - 7$ is within 1σ uncertainties, it might imply that the stellar population is slightly different between these galaxies. Shapley et al. (2003) have reported that the UV spectra of $z \sim 3$ LBGs become bluer with increasing $\text{Ly}\alpha$ equivalent width from large negative values (strong absorption) to large positive values (see also, Kornei et al. 2010). Similar trends have also been found for $z \sim 4$ LBGs by Pentericci et al. (2007), Vanzella et al. (2009), and Stark et al. (2010).

¹² http://data.spitzer.caltech.edu/popular/simple/20070601_enhanced/doc/OOREADME_photometry

¹³ The rest-frame wavelengths are 1580\AA and 1950\AA .

This trend might continue to $z \sim 6 - 7$, since there seems to be a hint of systematically bluer continua for LAEs than LBGs in Figure 2.

4. SED FITTING

Since LAEs tend to be young star-forming galaxies (e.g., Gawiser et al. 2007; Pirzkal et al. 2007; Lai et al. 2008; Ono et al. 2010), it is worthwhile to consider nebular emission in population synthesis modeling. Here we make model SEDs in two extreme cases: $f_{\text{esc}}^{\text{ion}} = 0$ where ionizing photons are totally converted into nebular emission, and $f_{\text{esc}}^{\text{ion}} = 1$ where all ionizing photons escape from the galaxy. We call the former the "stellar + nebular" case, and the latter the "pure stellar" case. We calculate nebular spectra (lines and continua) basically following the manner given in Schaerer & de Barros (2009).

We use the stellar population synthesis model of GALAXEV (Bruzual & Charlot 2003, hereafter BC03) to produce stellar SEDs¹⁴, adopting Salpeter's initial mass function (Salpeter 1955) with lower and upper mass cutoffs of 0.1 and $100M_{\odot}$. We assume constant star formation history¹⁵ and consider two stellar metallicities $Z = 0.2Z_{\odot}$ and $0.02Z_{\odot}$.

Nebular emission is calculated under the assumption of electron temperature $T_e = 10^4$ K, electron density $n_e = 10^2 \text{ cm}^{-3}$, and case B recombination. We include H recombination lines from Balmer, Paschen, and Brackett series¹⁶. We calculate H β line luminosity by (e.g., Osterbrock & Ferland 2006)

$$L(\text{H}\beta) [\text{erg s}^{-1}] = 4.78 \times 10^{-13} (1 - f_{\text{esc}}^{\text{ion}}) N_{\text{Lyc}}, \quad (2)$$

where N_{Lyc} is the number of ionizing photons produced per second. We do not consider absorption of ionizing photons by dust. The luminosities of the other H recombination lines are computed from $L(\text{H}\beta)$ using the table of relative intensities of these lines given in Storey & Hummer (1995). We also include nebular lines from non-hydrogens using the empirical relative line intensities compiled by Anders & Fritze-v. Alvensleben (2003), on the assumption that the gaseous metallicity is equal to the stellar metallicity.

Nebular continuum emission is calculated by (e.g., Krueger et al. 1995)

$$L_{\nu} = \frac{\gamma_{\nu}^{(\text{total})}}{\alpha_{\text{B}}} (1 - f_{\text{esc}}^{\text{ion}}) N_{\text{Lyc}}, \quad (3)$$

where α_{B} is the case B recombination coefficient for hydrogen. The continuum emission coefficient $\gamma_{\nu}^{(\text{total})}$, considering free-free and free-bound emission by H, neutral

He, and singly ionised He, as well as the two-photon continuum of H, is given by

$$\gamma_{\nu}^{(\text{total})} = \gamma_{\nu}^{(\text{HI})} + \gamma_{\nu}^{(2\text{q})} + \gamma_{\nu}^{(\text{HeI})} \frac{n(\text{He}^+)}{n(\text{H}^+)} + \gamma_{\nu}^{(\text{HeII})} \frac{n(\text{He}^{++})}{n(\text{H}^+)}. \quad (4)$$

The emission coefficients $\gamma_{\nu}^{(i)}$ ($i = \text{HI}, 2\text{q}, \text{HeI}, \text{HeII}$) for wavelengths below and above $1\mu\text{m}$ are taken from tables 4 – 9 of Aller (1984) and tables I and II of Ferland (1980), respectively¹⁷. The abundance ratios are set to be $n(\text{He}^+)/n(\text{H}^+) = 0.1$ and $n(\text{He}^{++})/n(\text{H}^+) = 0$ (e.g., Brown & Mathews 1970; Krueger et al. 1995).

For the dust extinction of output stellar spectra, we use Calzetti's extinction law (Calzetti et al. 2000) and vary $E(B - V)_{\star}$ as a free parameter over 0 and 1.50 with an interval of 0.01. For the dust extinction of nebular emission, we assume $E(B - V)_{\text{gas}} = E(B - V)_{\star}$ as proposed by Erb et al. (2006)¹⁸.

Note that we do not consider the effect of dust extinction on $f_{\text{esc}}^{\text{ion}}$. In other words, we assume that a Lyman continuum photon either ionizes a neutral hydrogen atom or escapes into the intergalactic medium through, e.g., holes in the gas. Dust extinction for Lyman continuum emission can substantially reduce the hydrogen-ionizing flux (e.g., Inoue 2001). However, the exact level of Lyman continuum extinction is difficult to assess even for galaxies in the local Universe, and much more so at higher redshifts (e.g., Zackrisson et al. 2008), although some authors suggest that the effect is very small for high-redshift galaxies (e.g., Gnedin et al. 2008; Razoumov & Sommer-Larsen 2010).

In Section 5.4, we place upper limits to $f_{\text{esc}}^{\text{ion}}$ from the minimum luminosity of nebular emission required to reproduce the observed SEDs. Those are regarded as conservative upper limits, since a non-zero fraction of Lyman continuum photons not converted into nebular emission will in practice be absorbed by dust before escaping into the IGM.

We perform the standard SED fitting method (for details, see Section 3 of Ono et al. 2010). We make a large set of stellar-mass-normalized model SEDs, varying age and dust extinction. We then redshift them to $z = 5.70$ and 6.56 and convolve them with bandpasses to calculate flux densities. For each object, we search for the best-fitting SED that minimizes χ^2 separately for $f_{\text{esc}}^{\text{ion}} = 0$ and 1 and separately for $Z = 0.2Z_{\odot}$ and $0.02Z_{\odot}$. Since stellar mass M_{star} is the amplitude of a model SED, we obtain the best-fitting M_{star} by solving $\partial\chi^2/\partial M_{\text{star}} = 0$. The errors in the best-fit SED parameters correspond to the 1σ confidence interval ($\Delta\chi^2 < 1$) for each parameter.

Since our i' -band flux density for the $z = 5.7$ LAE and z' -band flux density for the $z = 6.6$ LAE are contaminated from Ly α emission and IGM absorption, we use m_{con} calculated in Section 3.1 instead of these flux densities. We do not use short wavebands (i.e., BVR for $z = 5.7$ and $BVRi'$ for $z = 6.6$), since they suffer from the IGM absorption shortward of the Ly α wavelength,

¹⁴ We do not use new population synthesis models which include thermally pulsating asymptotic giant branch (TP-AGB) stars (e.g., Maraston 2005; Bruzual 2007), because LAEs tend to be very young and the contribution of TP-AGB stars should be negligible (e.g., Ono et al. 2010).

¹⁵ Since most LAEs are very young, constant star formation history (SFH) is a reasonable approximation. Younger ages will be obtained if exponentially decaying SFH is assumed, while older ages will be obtained for smoothly-rising SFH, which has been recently applied by several authors (e.g., Stark et al. 2009).

¹⁶ We do not include Ly α line, since Ly α photons are resonantly scattered by neutral hydrogen and its strength is quite uncertain. Instead, we derive the Ly α -free continuum magnitude m_{con} from i' - and $NB816$ -band photometry for the $z = 5.7$ LAE, and z' - and $NB921$ -band photometry for the $z = 6.6$ LAE, as described in Section 3.1.

¹⁷ We assume $\gamma_{\nu}^{(2\text{q})} = 0$ and $\gamma_{\nu}^{(\text{HeI})} = \gamma_{\nu}^{(\text{HI})}$ at $\lambda \geq 1\mu\text{m}$ (e.g., Schaerer & Vacca 1998).

¹⁸ We find that adopting $E(B - V)_{\text{gas}} = E(B - V)_{\star}/0.44$, which is proposed by Calzetti et al. (2000), does not significantly change our results.

the amount of which considerably differs among the lines of sight. Thus, model SEDs are fitted to the observed flux densities in $m_{\text{con}}, z', J, H, K, 3.6\mu\text{m}, 4.5\mu\text{m}, 5.8\mu\text{m}$, and $8.0\mu\text{m}$ -band for $z = 5.7$, and to the same bands except z' for $z = 6.6$. The free parameters in the fitting are stellar mass, age, and dust extinction. The degrees of freedom are six for $z = 5.7$ and five for $z = 6.6$.

5. RESULTS AND DISCUSSION

5.1. Stellar Populations of Lyman Alpha Emitters at $z \sim 6 - 7$

Table 2 summarizes the results of the SED fitting for our LAEs. First, we find that in both $f_{\text{esc}}^{\text{ion}} = 0$ and $f_{\text{esc}}^{\text{ion}} = 1$ the best-fit models for $Z = 0.2Z_{\odot}$ and $0.02Z_{\odot}$ are very similar to each other. This implies that the changes in the stellar and nebular emission spectra over $0.02 \lesssim Z/Z_{\odot} \lesssim 0.2$ are not large enough to significantly alter the best-fit parameters. In what follows we concentrate on the results for $Z = 0.2Z_{\odot}$ for simplicity.

Next, we find that the best-fit models are extremely different between $f_{\text{esc}}^{\text{ion}} = 0$ and 1. For $f_{\text{esc}}^{\text{ion}} = 0$ the best-fit models have relatively small stellar masses, $3 \times 10^7 M_{\odot}$ ($z = 5.7$) and $1 \times 10^8 M_{\odot}$ ($z = 6.6$), and young ages, 3 Myr ($z = 5.7$) and 1 Myr ($z = 6.6$). On the other hand, for $f_{\text{esc}}^{\text{ion}} = 1$ the stellar masses are more than one order of magnitude higher, $5 \times 10^8 M_{\odot}$ and $3 \times 10^9 M_{\odot}$, and the ages are more than two orders of magnitude older, 300 Myr and 800 Myr. As we see below, these great differences are related to how to account for the observed bright IRAC magnitudes, or equivalently the red UV-to-optical colors. In contrast to the stellar mass and age, the dust extinction is consistent with $E(B - V)_{\star} = 0$ in both cases for both objects, suggesting that typical LAEs at $z \sim 6 - 7$ are nearly free from dust extinction.

Figure 3 compares the best-fit model spectra with the observed flux densities. The bottom panels show the results for $f_{\text{esc}}^{\text{ion}} = 1$, the "pure stellar" case. For $z = 5.7$, the best-fit model matches the observation at $\lambda_{\text{obs}} \lesssim 2\mu\text{m}$ but undershoots the data point at $3.6\mu\text{m}$. This offset will be reduced if older ages or larger $E(B - V)_{\star}$ values are adopted, but such models will then not fit the blue UV spectra. The observed SED of the $z = 6.6$ LAE resembles that of the $z = 5.7$ LAE, with blue UV colors and detection at $3.6\mu\text{m}$. In addition, the $z = 6.6$ LAE has a relatively bright flux density at $4.5\mu\text{m}$ as well although less than 3σ detection. The overall shape of the $z = 6.6$ SED is reproduced well by a pure stellar model.

The top panels of Figure 3 show the results for $f_{\text{esc}}^{\text{ion}} = 0$, i.e., the "stellar + nebular" case. We find that for $z = 5.7$ the discrepancy at $3.6\mu\text{m}$ seen in the bottom panel almost disappears thanks to strong nebular emission lines such as [OIII] and $H\beta$ contributing to this bandpass; the stellar emission has only a minor contribution. Thus, adopting a very young stellar population with strong nebular emission can simultaneously fit the observed blue UV color and the red UV-to-optical color. For $z = 6.6$ as well, the best-fit model with $f_{\text{esc}}^{\text{ion}} = 0$ reproduces the observed SED well in a similar manner.

Then, which of $f_{\text{esc}}^{\text{ion}} = 1$ and $f_{\text{esc}}^{\text{ion}} = 0$ is more favored? For $z = 5.7$ it is easy to answer this question. As shown in Table 2, the best-fit χ^2 for $f_{\text{esc}}^{\text{ion}} = 0$, 7.75, is significantly smaller than that for $f_{\text{esc}}^{\text{ion}} = 1$, 10.3. Indeed, the $f_{\text{esc}}^{\text{ion}} = 0$ model fits the $3.6\mu\text{m}$ data point and blue $3.6\mu\text{m}$

– $4.5\mu\text{m}$ color far better than the $f_{\text{esc}}^{\text{ion}} = 1$ model. In addition, the small photometric errors in the m_{con}, z' , and J magnitudes do not permit old-age, high-mass models which fit the $3.6\mu\text{m}$ data but instead give red UV colors.

For $z = 6.6$, on the other hand, the best-fit $f_{\text{esc}}^{\text{ion}} = 1$ model gives almost the same χ^2 (2.9) as the $f_{\text{esc}}^{\text{ion}} = 0$ model (2.5), and we cannot conclude which is favored solely from the χ^2 values. This is partly because the larger photometric errors in the J and shorter band-passes, and flatter $3.6\mu\text{m} - 4.5\mu\text{m}$ color permit old, massive models with red UV colors. However, typical LAEs at $z \sim 3 - 5$ have been consistently found to be young and low-mass objects (e.g., Gawiser et al. 2007; Pirzkal et al. 2007; Lai et al. 2008; Ono et al. 2010), and our study shows that this trend continues at $z = 5.7$. Combining this fact with an argument that it seems unnatural that LAEs at earlier epochs are *older* and *more massive*, we take the model with $f_{\text{esc}}^{\text{ion}} = 0$ for the $z = 6.6$ LAE¹⁹.

We conclude that typical LAEs at $z \sim 6 - 7$ have low stellar masses of $\sim (3 - 10) \times 10^7 M_{\odot}$, very young ages of $\sim 1 - 3$ Myr, and negligible dust extinction. We thus propose that they are candidates of galaxy building blocks at an early stage of galaxy formation. This proposal can be regarded as an extension toward higher redshift of a similar idea which has been proposed for low-redshift LAEs based on apparent magnitudes and sizes (Pascarella et al. 1996 for $z \sim 2$; see also Ouchi et al. 2003 who found that $z \sim 5$ LAEs are UV faint) and stellar population analysis (Gawiser et al. 2007 for $z \sim 3$). This proposal is also consistent with low dark-halo masses estimated for LAEs from clustering analysis (Gawiser et al. 2007 for $z \sim 3$, Guaita et al. 2010 for $z \sim 2$, Ouchi et al. 2010 for $z \sim 3 - 7$).

5.2. Constraints on Ly α Escape Fraction

We estimate for our LAEs the Ly α escape fraction, $f_{\text{esc}}^{\text{Ly}\alpha}$, by:

$$f_{\text{esc}}^{\text{Ly}\alpha} = \frac{L_{\text{obs}}(\text{Ly}\alpha)}{L_{\text{int}}(\text{Ly}\alpha)}, \quad (5)$$

where $L_{\text{obs}}(\text{Ly}\alpha)$ is the observed Ly α luminosity and $L_{\text{int}}(\text{Ly}\alpha)$ is the intrinsic Ly α luminosity computed from the SFR on the assumption of case B using $L_{\text{int}}(\text{Ly}\alpha)$ [erg s^{-1}] = 1.1×10^{42} SFR [$M_{\odot} \text{ yr}^{-1}$] (Brocklehurst 1971; Kennicutt 1998). As is easily noticed, $f_{\text{esc}}^{\text{Ly}\alpha}$ corresponds to the fraction of Ly α photons produced in the galaxy which escape from absorption by the galaxy's ISM and absorption by the IGM at the galaxy's redshift. Because the dust extinction of our LAEs is negligibly small (Section 5.1), Ly α photons propagating in the ISM are mostly just scattered by HI gas without absorption. In this case, $f_{\text{esc}}^{\text{Ly}\alpha}$ depends mostly on the strength of the IGM absorption.

Substituting the observed Ly α luminosity and SFR derived from our SED fitting, we obtain $f_{\text{esc}}^{\text{Ly}\alpha} \simeq 0.36_{-0.35}^{+0.68}$ for $z = 5.7$ LAEs, and $f_{\text{esc}}^{\text{Ly}\alpha} \simeq 0.040_{-0.038}^{+1.8}$ for $z = 6.6$

¹⁹ We cannot completely rule out the possibility that due to some selection effect unique to the $z = 6.6$ sample, our $z = 6.6$ LAEs are biased toward very massive objects. However, such selection effects are very unlikely, since the $z = 6.6$ sample has been selected in a similar manner to the $z = 5.7$ sample from the same data set, and the stacked objects at these two redshifts have similar $L(\text{Ly}\alpha)$ and M_{UV} , as found in Table 1.

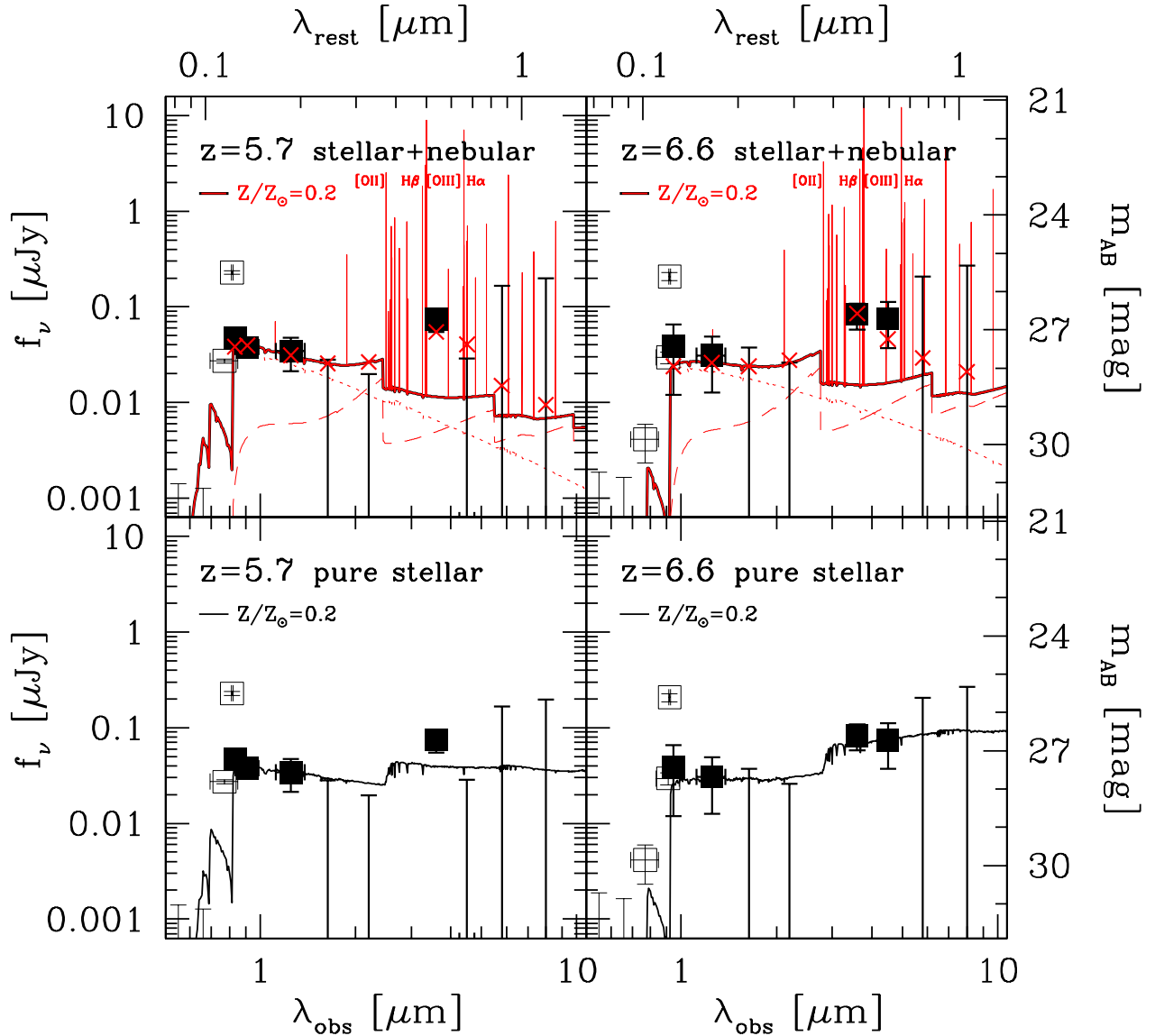


FIG. 3.— Best-fit SEDs (curves) and observed magnitudes (filled squares: used for SED fitting, open squares: not used) for the $z = 5.7$ LAE (left panels) and the $z = 6.6$ LAE (right panels). The top panels are for ‘stellar + nebular’ ($f_{\text{esc}}^{\text{ion}} = 0$) models. The red solid curves indicate the best-fit SEDs that are the sum of a stellar SED (red dotted curve) and a nebular SED (red dashed curve). The crosses indicate synthesized flux densities in individual bandpasses. The bottom panels are for ‘pure stellar’ ($f_{\text{esc}}^{\text{ion}} = 1$) models.

LAEs, as plotted in Figure 5. We find a tentative decrease in $f_{\text{esc}}^{\text{Ly}\alpha}$ from $z = 5.7$ to 6.6 . Ono et al. (2010) have found that LAEs at $z \sim 3 - 4$ have $f_{\text{esc}}^{\text{Ly}\alpha} \simeq 0.1 - 1$. Hayes et al. (2010) have obtained the median value of $f_{\text{esc}}^{\text{Ly}\alpha}$ for $z = 2.2$ LAEs to be higher than 0.32. These results might suggest that the Ly α escape fraction of LAEs is nearly constant up to 5.7, and then decreases toward $z = 6.6$. This decrease, if real, could be due to an increase with redshift in the hydrogen neutral fraction of the IGM, thereby Ly α photons are scattered more frequently. Indeed, a possible increase in the neutral fraction has been proposed from an observed decline in the number density of bright LAEs from $z = 5.7$ to $z = 6.6$ by Kashikawa et al. (2006).

Further discussion on the neutral fraction is, however, difficult given the quality of the $f_{\text{esc}}^{\text{Ly}\alpha}$ measurements. Note also that there may be some other mechanisms

which change $f_{\text{esc}}^{\text{Ly}\alpha}$. For example, unlike our assumption, Ly α emissivity at a given SFR might decrease from $z = 5.7$ to 6.6 . Although Figure 5 shows potential usefulness of $f_{\text{esc}}^{\text{Ly}\alpha}$ as a means to evaluate the IGM neutral fraction near the reionization epoch, much deeper multi-band photometry and more detailed SED modeling will be needed to obtain a reliable constraint.

5.3. Comparison with LBGs at $z \sim 7$

We fit model SEDs to a $z \sim 7$ z -dropout composed of 14 objects recently discovered by the HST/WFC3 survey (Oesch et al. 2010; Labbé et al. 2010), to compare with our LAEs. They have been selected from an extremely deep ($5\sigma \approx 28.6 - 28.7$ over $0.''25$ -radius apertures in Y_{105} , J_{125} , and H_{160}) area of 4.7 arcmin² using $z_{850} - Y_{105}$ and $Y_{105} - J_{125}$ colors and have an expected redshift distribution $z \sim 6.5 - 7.5$. We consider the observed

TABLE 2
SED FITTING RESULTS FOR THE LAEs AT $z = 5.7$ AND 6.6

model	Z [Z_{\odot}]	$\log M_{\text{star}}$ [M_{\odot}]	$E(B - V)_{\star}$ [mag]	$\log(\text{Age})$ [yr]	$\log(\text{SFR})$ [$M_{\odot} \text{ yr}^{-1}$]	$\log(\text{SSFR})$ [yr^{-1}]	χ^2
$z = 5.7$ LAE							
stellar + nebular	0.2	$7.49^{+0.20}_{-0.03}$	$0.00^{+0.03}_{-0.00}$	$6.50^{+0.62}_{-1.40}$	$0.99^{+1.48}_{-0.46}$	$-6.50^{+1.40}_{-1.78}$	7.75
pure stellar	0.2	$8.69^{+0.32}_{-0.56}$	$0.00^{+0.07}_{-0.00}$	$8.46^{+0.35}_{-0.91}$	$0.31^{+0.42}_{-0.02}$	$-8.38^{+1.80}_{-0.48}$	10.3
stellar + nebular	0.02	$7.49^{+0.37}_{-0.01}$	$0.00^{+0.05}_{-0.00}$	$6.62^{+0.58}_{-1.52}$	$0.87^{+1.63}_{-0.33}$	$-6.62^{+1.52}_{-2.13}$	9.00
pure stellar	0.02	$8.88^{+0.26}_{-0.39}$	$0.00^{+0.07}_{-0.00}$	$8.71^{+0.25}_{-0.55}$	$0.26^{+0.35}_{-0.01}$	$-8.61^{+1.13}_{-0.24}$	10.4
$z = 6.6$ LAE							
stellar + nebular	0.2	$7.95^{+1.66}_{-0.30}$	$0.11^{+0.24}_{-0.11}$	$5.95^{+2.96}_{-0.85}$	$2.00^{+1.21}_{-1.66}$	$-5.95^{+0.85}_{-2.86}$	2.53
pure stellar	0.2	$9.43^{+0.28}_{-0.33}$	$0.09^{+0.19}_{-0.09}$	$8.91^{+0.00}_{-0.95}$	$0.63^{+0.71}_{-0.24}$	$-8.81^{+2.33}_{-0.00}$	2.86
stellar + nebular	0.02	$8.07^{+1.63}_{-0.30}$	$0.13^{+0.25}_{-0.11}$	$6.38^{+2.53}_{-1.28}$	$1.69^{+1.63}_{-1.27}$	$-6.38^{+1.28}_{-2.42}$	2.46
pure stellar	0.02	$9.57^{+0.28}_{-0.32}$	$0.14^{+0.20}_{-0.11}$	$8.91^{+0.00}_{-0.85}$	$0.77^{+0.74}_{-0.28}$	$-8.80^{+2.26}_{-0.00}$	3.05

TABLE 3
SED FITTING RESULTS FOR THE $z \sim 7$ z -DROPOUT GALAXY

model	Z [Z_{\odot}]	$\log M_{\text{star}}$ [M_{\odot}]	$E(B - V)_{\star}$ [mag]	$\log(\text{Age})$ [yr]	$\log(\text{SFR})$ [$M_{\odot} \text{ yr}^{-1}$]	$\log(\text{SSFR})$ [yr^{-1}]	χ^2
$z \sim 7$ z -dropout							
stellar + nebular	0.2	$7.72^{+0.10}_{-0.18}$	$0.04^{+0.03}_{-0.04}$	$6.16^{+0.52}_{-1.06}$	$1.56^{+1.16}_{-0.68}$	$-6.16^{+1.06}_{-0.94}$	7.35
		$8.83^{+0.22}_{-0.30}$	$0.00^{+0.01}_{-0.00}$	$8.61^{+0.25}_{-0.35}$	$0.31^{+0.05}_{-0.01}$	$-8.52^{+0.67}_{-0.24}$	6.90
pure stellar	0.2	$8.98^{+0.12}_{-0.27}$	$0.00^{+0.01}_{-0.00}$	$8.76^{+0.10}_{-0.30}$	$0.32^{+0.05}_{-0.00}$	$-8.66^{+0.43}_{-0.10}$	6.26

NOTE. — For the $z \sim 7$ z -dropout, shown are two equally well fitted $f_{\text{esc}}^{\text{ion}} = 0$ models, a very young model and a very old model. See text for details.

flux densities in the z_{850} , Y_{105} , J_{125} , H_{160} , K , $3.6\mu\text{m}$, $4.5\mu\text{m}$ band taken from Table 1 of Labbé et al. (2010), assuming a redshift of $z = 6.88$, which is derived by Labbé et al. (2010). This stacked object is similarly faint in the rest UV continuum ($J_{125} = 29.6$) to our LAEs, and thus suitable for comparison. We do not use two z -dropout candidates reported by Capak et al. (2009) and 11 $z_{850\text{LP}}$ -dropouts discovered by González et al. (2010), because they are too bright (the former have $J \sim 23$ and the latter $J_{110\text{W}} \sim 26 - 27.5$). In our SED fitting, we rule out the i_{775} -band data although Labbé et al. (2010) used it for their SED fitting, since it suffers from the IGM absorption shortward of Ly α wavelength, and the amount of the absorption differs with the line of sight. The free parameters are thus stellar mass, age, and dust extinction, and the degrees of freedom are four.

This object has also been SED-fitted by Schaerer & de Barros (2010), using stellar population synthesis models with nebular emission. The major difference between their and our modelings are the star formation history assumed. Schaerer & de Barros (2010) have assumed an exponentially declining star formation rate with its e -folding time as a free parameter, while we assume a constant star formation rate. For a fair comparison with our results on LAEs, we reanalyze the z -dropout SED with our models. The best-fit parameters are given in Table 2.

The bottom panel of Figure 6 shows the result for $f_{\text{esc}}^{\text{ion}} = 1$. We find that the observed SED is well explained by a low-mass ($\log(M_{\text{star}}[M_{\odot}]) = 8.98^{+0.12}_{-0.27}$) and

moderately aged ($\log(\text{Age}[\text{yr}]) = 8.76^{+0.10}_{-0.30}$) model with little dust extinction ($E(B - V)_{\star} = 0.00^{+0.01}_{-0.00}$)²⁰. This result is consistent with that of Labbé et al. (2010) who examined $f_{\text{esc}}^{\text{ion}} = 1$ models alone.

The top panel of Figure 6 shows the result for $f_{\text{esc}}^{\text{ion}} = 0$. We obtain almost the same parameters as the $f_{\text{esc}}^{\text{ion}} = 1$ model: $\log(M_{\text{star}}[M_{\odot}]) = 8.83^{+0.22}_{-0.30}$, $\log(\text{Age}[\text{yr}]) = 8.61^{+0.25}_{-0.35}$, and $E(B - V)_{\star} = 0.00^{+0.01}_{-0.00}$. However, we find that the data are also well reproduced by a low-mass ($\log(M_{\text{star}}[M_{\odot}]) = 7.72^{+0.07}_{-0.11}$), extremely young ($\log(\text{Age}[\text{yr}]) = 6.16^{+0.30}_{-1.06}$), and almost extinction free ($E(B - V)_{\star} = 0.04^{+0.02}_{-0.03}$) model, which are also shown in Table 2. Although these two models are extremely different, they have almost the same χ^2 values, and we cannot conclude which is more favored. In summary, the z -dropout galaxy is either a very young, low-mass object, or a very old, massive object. To be interesting, just like in the case of the $z = 6.6$ LAEs, models with intermediate ages and masses are not favored.

If we take account of the difference in the assumed star formation history, our results are broadly consistent with those of Schaerer & de Barros (2010). As shown in Figure C.2 of their paper, they have derived two equally-fitted solutions: very young (~ 4 Myr) and old (~ 700

²⁰ The age suggests that the formation redshift of this object is ≥ 9.5 .

²¹ The age suggests that the formation redshift of this object is ≥ 8.5 .

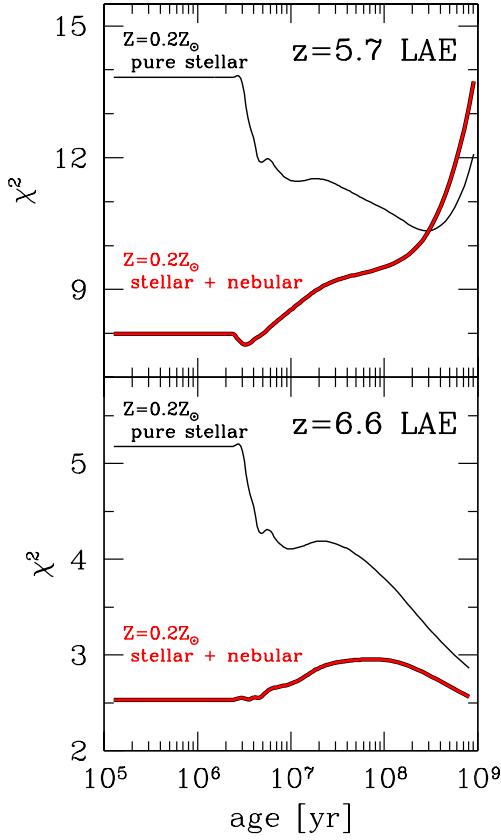


FIG. 4.— χ^2 of the best-fit model as a function of age (top: $z = 5.7$ LAE, bottom: $z = 6.6$ LAE). The red curves are for $f_{\text{esc}}^{\text{ion}} = 0$ and the black curves for $f_{\text{esc}}^{\text{ion}} = 1$.

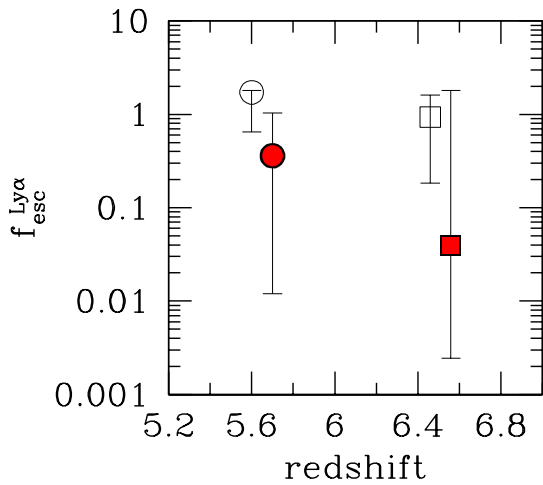


FIG. 5.— $\text{Ly}\alpha$ escape fraction as a function of redshift. The circles (squares) correspond to $z = 5.7$ (6.6). The filled and open symbols are for $f_{\text{esc}}^{\text{ion}} = 0$ and 1 , respectively, where the open symbols have been shifted by -0.1 along the x -axis for clarity. Although $f_{\text{esc}}^{\text{ion}} = 1$ is physically unrealistic because $\text{Ly}\alpha$ photons cannot be produced, we plot the results to show how $f_{\text{esc}}^{\text{Ly}\alpha}$ varies with $f_{\text{esc}}^{\text{ion}}$ in our method.

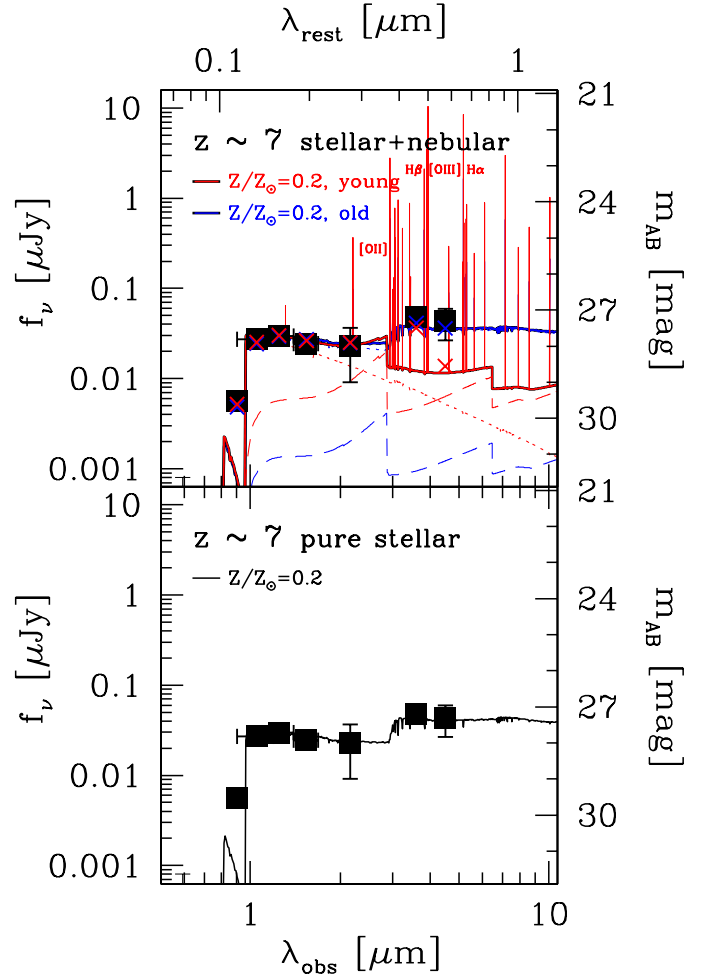


FIG. 6.— Same as Figure 3, but for the $z \sim 7$ z -dropout galaxy (Labbé et al. 2010). In the top panel, two equally well fitted $f_{\text{esc}}^{\text{ion}} = 0$ models are plotted: the ‘young’ model in red and the ‘old’ model in blue.

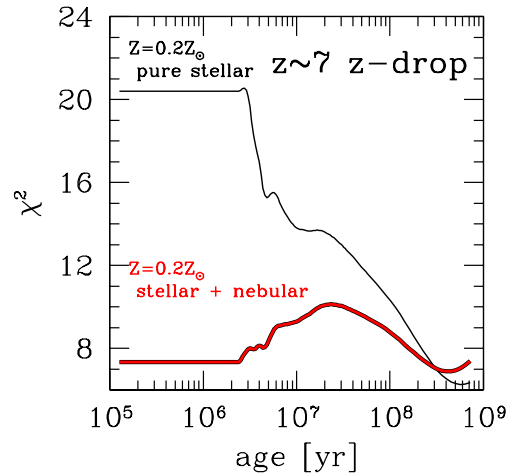


FIG. 7.— Same as Figure 4, but for the $z \sim 7$ z -dropout galaxy (Labbé et al. 2010).

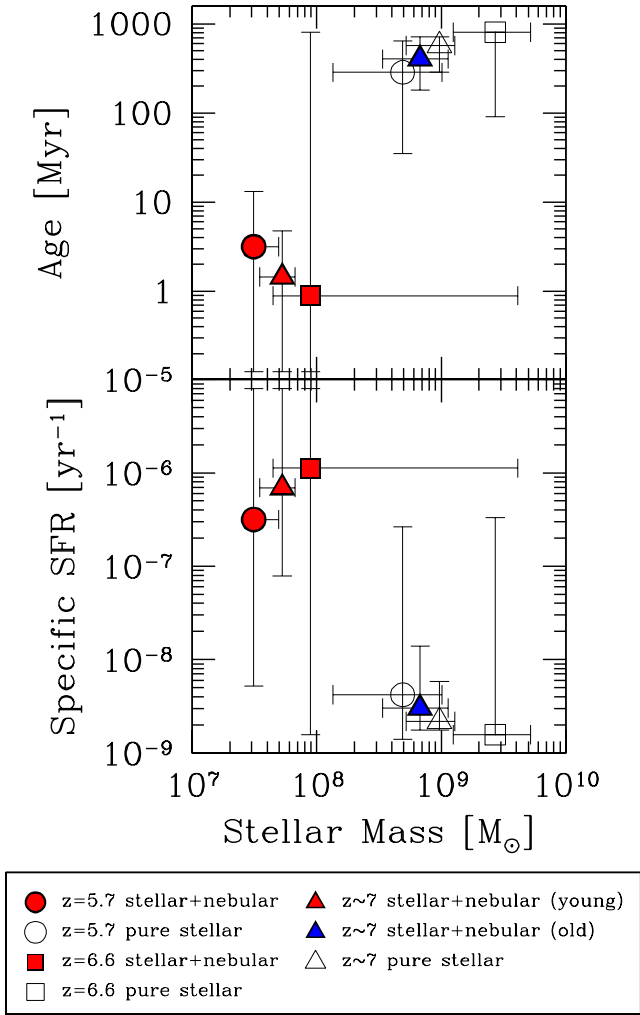


FIG. 8.— **Top panel:** age versus stellar mass M_{star} . The circles, squares, and triangles are for the $z = 5.7$ LAE, $z = 6.6$ LAE, and $z \sim 7$ dropout galaxy (Labbé et al. 2010), respectively. The results for $f_{\text{esc}}^{\text{ion}} = 0$ are colored in red, while those for $f_{\text{esc}}^{\text{ion}} = 1$ are shown in open symbols. For the $z \sim 7$ dropout galaxy, we also plot the old $f_{\text{esc}}^{\text{ion}} = 0$ model in blue. **Bottom panel:** specific star formation rate (SSFR = $\text{SFR}/M_{\text{star}}$) versus stellar mass M_{star} . The symbols are the same as in the top panel.

Myr). Note that their χ^2 values do not match with ours. This would be because they have parameterized the star-formation e -folding time and metallicity, which we fix, as well, and they have considered B_{435} , V_{606} , and i_{775} data, which we do not consider.

The top panel of Figure 8 plots the best-fit age against the best-fit M_{star} for our LAEs and the $z \sim 7$ z -dropout. The best-fit solutions for our $z = 5.7$ and 6.6 LAEs (red filled circle and square) suggest that they are low-mass and very young star-forming galaxies. As for the $z \sim 7$ z -dropout, both of the two extreme solutions (red and blue filled triangles) are plotted. If the younger solution is true, the z -dropout is as old and massive as our LAEs. On the other hand, if the older solution is true, the z -dropout is much older and more massive than our LAEs.

The bottom panel of Figure 8 shows the specific SFR (SSFR) as a function of M_{star} . Our $z = 5.7$ and 6.6 LAEs have low stellar masses and very high SSFRs. On the other hand, the z -dropout has either almost the same

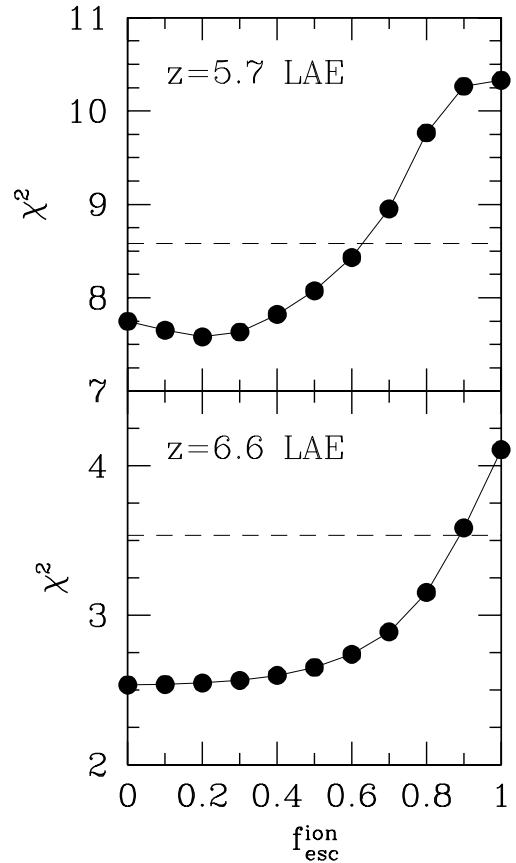


FIG. 9.— χ^2 versus the Lyman-continuum escape fraction $f_{\text{esc}}^{\text{ion}}$ for the $z = 5.7$ LAE (top panel) and the $z = 6.6$ LAE (bottom panel). The dashed lines correspond to $\chi_{\text{min}}^2 + 1$.

M_{star} and SSFR as the LAEs, or far more massive and lower SSFR than the LAEs.

5.4. Constraints on Ly Continuum Escape Fraction

In the previous sections we consider two extreme values for the Ly continuum escape fraction: $f_{\text{esc}}^{\text{ion}} = 1$ (pure stellar) and $f_{\text{esc}}^{\text{ion}} = 0$ (stellar + nebular). Indeed, our data are not deep enough to place as a strong constraint on $f_{\text{esc}}^{\text{ion}}$ as on the other parameters. However, since $f_{\text{esc}}^{\text{ion}}$ is a very important quantity which controls cosmic reionization, in this subsection we perform SED fitting with $f_{\text{esc}}^{\text{ion}}$ as an additional free parameter, to try to obtain rough constraints on $f_{\text{esc}}^{\text{ion}}$. We vary $f_{\text{esc}}^{\text{ion}}$ over 0 and 1 with an interval of 0.1. In the fitting of the $z = 6.6$ LAE, we search for the best-fit age in the range of < 20 Myr following the argument in Section 5.1 that the $z = 6.6$ LAE is likely to be very young.

Figure 9 shows χ^2 as a function of $f_{\text{esc}}^{\text{ion}}$ for our LAEs. For $z = 5.7$, χ^2 is nearly constant up to $f_{\text{esc}}^{\text{ion}} = 0.5$ and then starts to increase. Beyond $f_{\text{esc}}^{\text{ion}} \sim 0.6$ it exceeds $\chi_{\text{min}}^2 + 1$, the 1σ confidence level. We can thus place an upper limit of $f_{\text{esc}}^{\text{ion}} \sim 0.6$. For $z = 6.6$, χ^2 changes little up to as high as $f_{\text{esc}}^{\text{ion}} = 0.8$, and exceeds $\chi_{\text{min}}^2 + 1$ at around 0.9. Thus $f_{\text{esc}}^{\text{ion}}$ is only loosely constrained as $f_{\text{esc}}^{\text{ion}} \lesssim 0.9$. We also do a similar analysis to the z -dropout but obtain no meaningful constraint, since χ^2 does not change larger than unity over the whole $f_{\text{esc}}^{\text{ion}}$ range. This

TABLE 4
 SED FITTING RESULTS FOR THE LAEs AT $z = 5.7$ AND 6.6

model	Z [Z_{\odot}]	$\log M_{\text{star}}$ [M_{\odot}]	$E(B-V)_{\star}$ [mag]	$\log(\text{Age})$ [yr]	$\log(\text{SFR})$ [$M_{\odot} \text{ yr}^{-1}$]	$\log(\text{SSFR})$ [yr^{-1}]	χ^2
$z = 5.7$ LAE							
$f_{\text{esc}}^{\text{ion}} = 0.2$	0.2	$7.55^{+0.15}_{-0.08}$	$0.00^{+0.04}_{-0.00}$	$5.95^{+0.91}_{-0.85}$	$1.60^{+0.96}_{-0.92}$	$-5.95^{+0.85}_{-2.24}$	7.58
$z = 6.6$ LAE							
$f_{\text{esc}}^{\text{ion}} = 0.2$	0.2	$8.08^{+0.81}_{-0.28}$	$0.14^{+0.23}_{-0.11}$	$5.95^{+1.41}_{-0.85}$	$2.13^{+1.23}_{-1.04}$	$-5.95^{+0.85}_{-1.38}$	2.55

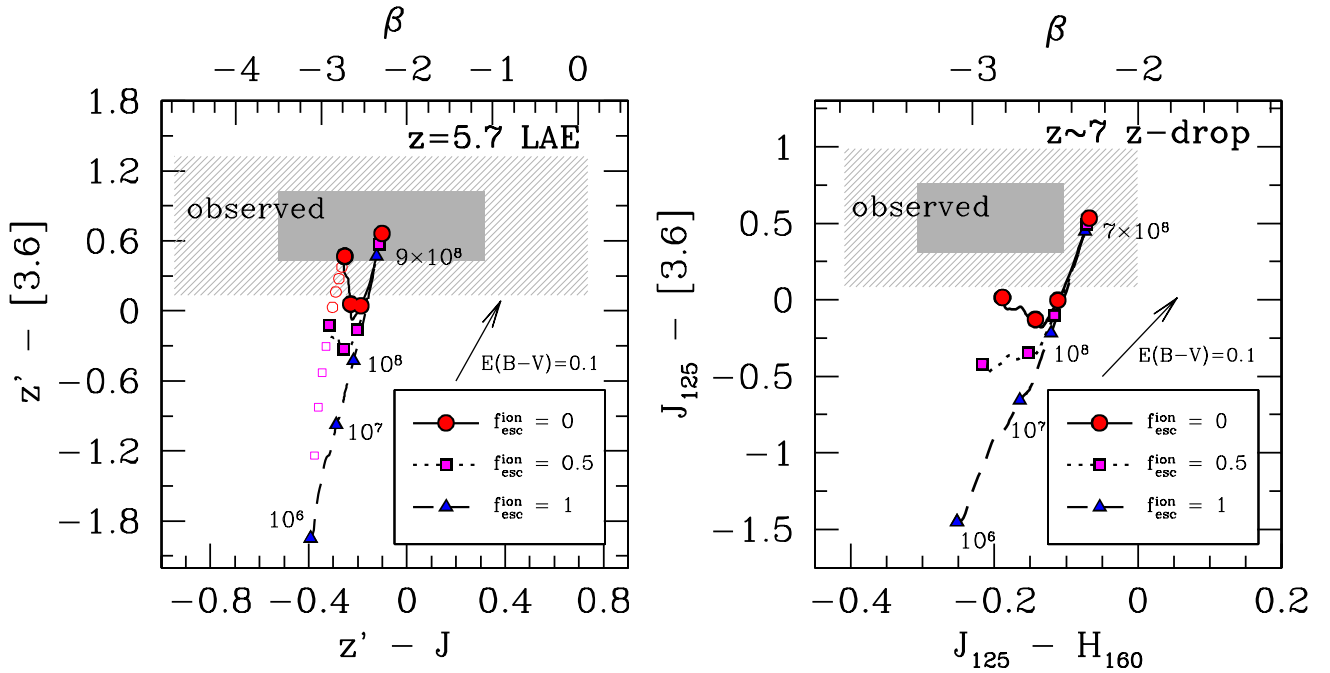


FIG. 10.— **Left panel:** comparison of the observed $z' - [3.6]$ versus $z' - J$ of the $z = 5.7$ LAE (shaded region: 1σ range; hatched region: 2σ range) with model tracks from $\simeq 10^6$ yr to 9×10^8 yr with $Z = 0.2Z_{\odot}$ and a constant star formation rate, for $f_{\text{esc}}^{\text{ion}} = 0$ (solid curve with red circles corresponding to four ages: 10^6 , 10^7 , 10^8 , 9×10^8 yr from left to right), 0.5 (dotted curve with magenta squares), and 1 (dashed curve with blue triangles). The open symbols represent $\simeq 10^6$ yr models with $f_{\text{esc}}^{\text{ion}} = 0.1 - 0.4$ (red open circles) and $f_{\text{esc}}^{\text{ion}} = 0.6 - 0.9$ (magenta open squares) from top to bottom. The arrow shows the effects of dust extinction on model colors (Calzetti et al. 2000). **Right panel:** comparison of the observed $J_{125} - [3.6]$ versus $J_{125} - H_{160}$ of the $z \sim 7$ z-dropout (Labbé et al. 2010) (shaded region: 1σ range; hatched region: 2σ range) with model tracks from $\simeq 10^6$ yr to 7×10^8 yr with $Z = 0.2Z_{\odot}$ and a constant star formation rate, for $f_{\text{esc}}^{\text{ion}} = 0$ (solid curve with red circles corresponding to four ages: $\simeq 10^6$, 10^7 , 10^8 , 7×10^8 yr from left to right), 0.5 (dotted curve with magenta squares), and 1 (dashed curve with blue triangles). The arrow shows the effects of dust extinction on model colors (Calzetti et al. 2000).

is probably because the z -dropout is fit well by an old-age model as well (see Section 5.3) in which nebular emission is so weak that χ^2 is insensitive to $f_{\text{esc}}^{\text{ion}}$. If we limit the age of the z -dropout to < 20 Myr, as in the case of the $z = 6.6$ LAE, then we obtain an upper limit of $f_{\text{esc}}^{\text{ion}} \sim 0.2$.

Although our LAE data cannot strongly constrain $f_{\text{esc}}^{\text{ion}}$, it would be worth presenting the best-fit results for $f_{\text{esc}}^{\text{ion}} = 0.2$, at which χ^2 for the $z = 5.7$ LAE reaches its minimum. As found in Table 4, the best-fit parameters for $f_{\text{esc}}^{\text{ion}} = 0.2$ overlap well with those for $f_{\text{esc}}^{\text{ion}} = 0$ (Table 2) within the errors, indicating that our conclusions on the stellar populations obtained in Section 5.1 are relatively robust against the uncertainty in $f_{\text{esc}}^{\text{ion}}$.

The reason for $f_{\text{esc}}^{\text{ion}}$ having an upper limit is that with too large $f_{\text{esc}}^{\text{ion}}$, young stellar populations favored by the

observed blue UV continua cannot produce nebular emission strong enough to account for the observed red UV-to-optical color. In this sense, the UV-to-optical color is critical to constrain $f_{\text{esc}}^{\text{ion}}$. We explain this situation using Figure 10. In this figure, three model tracks for the $z = 5.7$ LAE over ages of 10^6 to 9×10^8 yr are plotted according to three $f_{\text{esc}}^{\text{ion}}$ values, 0, 0.5, 1, in the $z' - [3.6]$ versus $z' - J$ plane. We take $z' - J$ as a representative of the rest-frame UV color and $z' - [3.6]$ as a rest-frame UV-to-optical color bracketing 4000 \AA . The shaded and hatched regions are, respectively, the observationally permitted 1σ and 2σ ranges. The $z' - J$ color at a fixed age becomes bluer with $f_{\text{esc}}^{\text{ion}}$ but the change is modest. In contrast, $z' - [3.6]$ increases with $f_{\text{esc}}^{\text{ion}}$ very sensitively for young ages. For example, for an age of 10^6 yr, which is

close to the best-fit age of the $z = 5.7$ LAE, $z' - [3.6]$ becomes rapidly redder with $f_{\text{esc}}^{\text{ion}}$ (magenta squares) and the model goes out of the hatched region at $f_{\text{esc}}^{\text{ion}} \sim 0.3$. Although the goodness of models should be measured using the all magnitude data, this figure demonstrates the importance of a UV-to-optical color in constraining $f_{\text{esc}}^{\text{ion}}$.

Recently, Bouwens et al. (2010b) proposed that the very blue UV color of z -dropout galaxies they found may be due to weak nebular emission and hence high $f_{\text{esc}}^{\text{ion}}$, because strong nebular emission makes the UV color too red. However, as they already state, $f_{\text{esc}}^{\text{ion}}$ is not uniquely determined from the UV color but it also depends on the age of the stellar population. Inclusion of a UV-to-optical color greatly reduces this age- $f_{\text{esc}}^{\text{ion}}$ degeneracy, as illustrated in Figure 10. Basically, with very accurate measurements of a UV color and a UV-to-optical color, we can obtain a stringent constraint on $f_{\text{esc}}^{\text{ion}}$ (for a fixed metallicity and IMF). For instance, if β of the z -dropout was found to be -3 with a great accuracy, low $f_{\text{esc}}^{\text{ion}}$ models such as $f_{\text{esc}}^{\text{ion}} = 0$ would be ruled out. On the other hand, if β and $J_{125} - [3.6]$ of the z -dropout were found to be -2.8 and 0 respectively, with great accuracies, low $f_{\text{esc}}^{\text{ion}}$ models would be favored.

Several studies have recently constrained lower limits of the escape fraction based on the UV luminosity density of z -dropout galaxies; Ouchi et al. (2009b) have obtained $f_{\text{esc}}^{\text{ion}} \gtrsim 0.2$, and Finkelstein et al. (2010) have obtained $f_{\text{esc}}^{\text{ion}} \gtrsim 0.3$. The upper limits obtained above complement these lower limits, thus narrowing the range permitted.

Several theoretical studies have argued that $f_{\text{esc}}^{\text{ion}}$ could vary depending on their host dark halo masses. However, there is no consensus on this tendency; Wise & Cen (2009) have reported that $f_{\text{esc}}^{\text{ion}}$ decreases as the halo mass decreases, while Razoumov & Sommer-Larsen (2010) have shown an opposite tendency (see also, Yajima et al. 2010). This controversy may be resolved if our method is applied to objects in a wide mass range.

5.5. Contribution of LAEs to the Stellar Mass Density and the Cosmic Star Formation Rate Density

We estimate the contribution from LAEs to the cosmic stellar mass density by dividing the total stellar mass of LAEs by the comoving volume searched by each narrow band. The total stellar mass at each redshift is defined as the stellar mass of the stacked LAEs multiplied by their number. Assuming $f_{\text{esc}}^{\text{ion}} = 0$, we obtain $\simeq 8.5 \times 10^3 [M_{\odot} \text{ Mpc}^{-3}]$ for $z = 5.7$ LAEs and $\simeq 1.6 \times 10^4 [M_{\odot} \text{ Mpc}^{-3}]$ for $z = 6.6$ LAEs. These values should be taken as lower limits, since we have excluded objects detected and/or significantly confused by neighboring objects in the $3.6\mu\text{m}$ image.

Eyles et al. (2007) have summed up the stellar masses of the i -drop galaxies they detected, to obtain a lower limit to the stellar mass density of $z \sim 6$ galaxies of $\sim 3 \times 10^6 [M_{\odot} \text{ Mpc}^{-3}]$. Stark et al. (2009) have derived the mass function of i' -dropout galaxies and obtained a stellar mass density of $\simeq 4.9 \times 10^6 [M_{\odot} \text{ Mpc}^{-3}]$ by integrating the mass function brightward of $M_{1500} = -20$. The stellar mass density of our $z = 5.7$ LAEs is only $\sim 0.2 - 0.3\%$ of these values.

For $z \sim 7$ galaxies, Labbé et al. (2010) have obtained a lower limit of $\sim 3.7 \times 10^6 [M_{\odot} \text{ Mpc}^{-3}]$ by multiplying the UV luminosity density of z -dropout galaxies

given in Bouwens et al. (2010a) by an estimated mass-to-luminosity ratio. Again, the stellar mass density of our $z = 6.6$ LAEs is as low as $\sim 0.4\%$ of this value.

Using SED fitting similar to ours, Ono et al. (2010) have obtained $1.4 \times 10^5 [M_{\odot} \text{ Mpc}^{-3}]$ for $z = 3.1$ LAEs, and $5.2 \times 10^5 [M_{\odot} \text{ Mpc}^{-3}]$ for $z = 3.7$ LAEs. These values are about 10–60 times larger than those of $z = 5.7$ and 6.6 LAEs, although they assumed $f_{\text{esc}}^{\text{ion}} = 1$.

Similarly, we estimate the contribution from LAEs to the cosmic star formation rate density (SFRD), where the total star formation rate is computed as the star formation rate of the stacked objects multiplied by their number. We obtain $\simeq 2.7 \times 10^{-3} [M_{\odot} \text{ yr}^{-1} \text{ Mpc}^{-3}]$ for $z = 5.7$ LAEs and $\simeq 1.8 \times 10^{-2} [M_{\odot} \text{ yr}^{-1} \text{ Mpc}^{-3}]$ for $z = 6.6$ LAEs. These values are also lower limits to the total stellar mass density of LAEs.

Bouwens et al. (2007) have estimated the SFRD of $z \sim 6$ galaxies to be $\sim 7.2 \times 10^{-3} [M_{\odot} \text{ yr}^{-1} \text{ Mpc}^{-3}]$ by integrating the UV luminosity function of i -dropout galaxies. Similarly, Ouchi et al. (2009b) have obtained $\sim 7.5 \times 10^{-3} [M_{\odot} \text{ yr}^{-1} \text{ Mpc}^{-3}]$ for $z \sim 7$ galaxies from the UV luminosity function of z -dropout galaxies (see also, Bouwens et al. 2010a). These two values are comparable to the lower limits obtained for our LAEs at $z = 5.7$ and 6.6 , suggesting that LAEs are major sources of the cosmic star formation at $z \sim 6 - 7$. Ono et al. (2010) have obtained $\simeq 8.2 \times 10^{-3} [M_{\odot} \text{ yr}^{-1} \text{ Mpc}^{-3}]$ for $z = 3.1$ LAEs, and $\simeq 1.3 \times 10^{-1} [M_{\odot} \text{ yr}^{-1} \text{ Mpc}^{-3}]$ for $z = 3.7$ LAEs. These values are about 0.5–50 times larger than those of $z = 5.7$ and 6.6 LAEs.

6. CONCLUSIONS

In this paper, we investigated the stellar populations of LAEs at $z = 5.7$ and 6.6 found in 0.65 deg^2 of the SXDF, based on deep rest-frame UV-to-optical photometry obtained from the three surveys: SXDS, UKIDSS/UDS, and SpUDS. We made composite images from 165 and 91 LAEs at $z = 5.7$ and 6.6 , respectively, which are fainter than the 3σ magnitude in the IRAC $3.6\mu\text{m}$ band, and derived typical SEDs of $z \sim 6 - 7$ LAEs for the first time. We found that their UV continua are as blue as those of dropout galaxies at similar redshifts, with UV spectral slopes $\beta \sim -3$, albeit with large photometric uncertainties. Fitting stellar population synthesis models with and without nebular emission, which is parameterized by $f_{\text{esc}}^{\text{ion}}$, to the multiband data of the stacked objects at $z = 5.7$ and 6.6 , we derived their stellar masses, ages, and dust extinction.

Our main results are as follows:

- (i) We find that the stacked LAEs at both redshifts are fitted well by $f_{\text{esc}}^{\text{ion}} = 0$ models. The best-fit $f_{\text{esc}}^{\text{ion}} = 0$ models have low stellar masses of $\sim (3 - 10) \times 10^7 M_{\odot}$, very young ages of $\sim 1 - 3$ Myr, and negligible dust extinction. In these models, young stellar populations reproduce the observed blue UV continua, and strong nebular emission redward of 4000 \AA makes the UV-to-optical color as red as observed.

While we find that the $z = 6.6$ LAE is also fitted similarly well by an old, massive model without nebular emission, we do not take this models as

the best-fit model, since typical LAEs up to $z \sim 6$, including our $z = 5.7$ LAEs, have been consistently found to be very young and low-mass galaxies. We propose that typical $z \sim 6 - 7$ LAEs are candidates of galaxy building blocks at the early stage of galaxy formation.

- (ii) We estimate the Ly α escape fraction to be $f_{\text{esc}}^{\text{Ly}\alpha} \simeq 0.36$ for the $z = 5.7$ LAE and $f_{\text{esc}}^{\text{Ly}\alpha} \simeq 0.04$ for the $z = 6.6$ LAE with large errors. This decrease from $z = 5.7$ to 6.6, if real, might be due to an increase in the neutral fraction of the IGM.
- (iii) We also apply SED fitting to a stacked object from $z \sim 7$ z -dropout galaxy candidates found by a recent HST/WFC3 deep survey, and find that it is either a young, low-mass galaxy with strong nebular emission similar to the $z = 5.7$ and 6.6 LAEs,

or a very old and massive galaxy with little nebular emission.

- (iv) From the constraints on nebular emission models, we estimate the upper limit of the Ly-continuum escape fraction to be $f_{\text{esc}}^{\text{ion}} \sim 0.6$ for the $z = 5.7$ LAE and ~ 0.9 for the $z = 6.6$ LAE. We apply this technique to the z -dropout galaxies, but obtain no meaningful constraints on $f_{\text{esc}}^{\text{ion}}$.

ACKNOWLEDGEMENTS

We would like to thank the anonymous referee for helpful comments and suggestions. We also thank Jason Kalirai for kindly providing the data; Daniel Schaerer, Richard Ellis, Andrea Ferrara, Eric Gawiser, and Daniel Stark for useful conversation. M.O. has been supported via Carnegie Fellowship. JSD and RJM thank the Royal Society for support via a Wolfson Research Merit Award and a University Research Fellowship respectively.

REFERENCES

- Aller, L. H., ed. 1984, *Astrophysics and Space Science Library*, Vol. 112, Physics of thermal gaseous nebulae
- Anders, P., & Fritze-v. Alvensleben, U. 2003, *A&A*, 401, 1063
- Becker, G. D., Rauch, M., & Sargent, W. L. W. 2007, *ApJ*, 662, 72
- Bouwens, R. J., Illingworth, G. D., Franx, M., & Ford, H. 2007, *ApJ*, 670, 928
- Bouwens, R. J., et al. 2009, *ApJ*, 705, 936
- . 2010a, *ApJ*, 709, L133
- . 2010b, *ApJ*, 708, L69
- Brocklehurst, M. 1971, *MNRAS*, 153, 471
- Brown, R. L., & Mathews, W. G. 1970, *ApJ*, 160, 939
- Bruzual, G. 2007, in *Astronomical Society of the Pacific Conference Series*, Vol. 374, *From Stars to Galaxies: Building the Pieces to Build the Universe*, ed. A. Vallenari, R. Tantalò, L. Portinari, & A. Moretti, 303–+
- Bruzual, G., & Charlot, S. 2003, *MNRAS*, 344, 1000
- Calzetti, D., Armus, L., Bohlin, R. C., Kinney, A. L., Koornneef, J., & Storchi-Bergmann, T. 2000, *ApJ*, 533, 682
- Capak, P., et al. 2009, *ArXiv e-prints* (arXiv:0910.0444)
- Casali, M., et al. 2007, *A&A*, 467, 777
- Chary, R., Stern, D., & Eisenhardt, P. 2005, *ApJ*, 635, L5
- Chen, H., Prochaska, J. X., & Gnedin, N. Y. 2007, *ApJ*, 667, L125
- Dawson, S., Rhoads, J. E., Malhotra, S., Stern, D., Wang, J., Dey, A., Spinrad, H., & Jannuzi, B. T. 2007, *ApJ*, 671, 1227
- Erb, D. K., Steidel, C. C., Shapley, A. E., Pettini, M., Reddy, N. A., & Adelberger, K. L. 2006, *ApJ*, 647, 128
- Eyles, L. P., Bunker, A. J., Ellis, R. S., Lacy, M., Stanway, E. R., Stark, D. P., & Chiu, K. 2007, *MNRAS*, 374, 910
- Fan, X., et al. 2006, *AJ*, 132, 117
- Fazio, G. G., et al. 2004, *ApJS*, 154, 10
- Ferland, G. J. 1980, *PASP*, 92, 596
- Finkelstein, S. L., Papovich, C., Gialalisco, M., Reddy, N. A., Ferguson, H. C., Koekemoer, A. M., & Dickinson, M. 2010, *ApJ*, 719, 1250
- Finkelstein, S. L., Rhoads, J. E., Malhotra, S., & Grogin, N. 2009, *ApJ*, 691, 465
- Furusawa, H., et al. 2008, *ApJS*, 176, 1
- Fynbo, J. P. U., et al. 2009, *ApJS*, 185, 526
- Gawiser, E., et al. 2007, *ApJ*, 671, 278
- Gnedin, N. Y., Kravtsov, A. V., & Chen, H. 2008, *ApJ*, 672, 765
- González, V., Labbé, I., Bouwens, R. J., Illingworth, G., Franx, M., Kriek, M., & Brammer, G. B. 2010, *ApJ*, 713, 115
- Gronwall, C., et al. 2007, *ApJ*, 667, 79
- Guaita, L., et al. 2010, *ApJ*, 714, 255
- Hayes, M., et al. 2010, *Nature*, 464, 562
- Hewett, P. C., Warren, S. J., Leggett, S. K., & Hodgkin, S. T. 2006, *MNRAS*, 367, 454
- Hu, E. M., Cowie, L. L., & McMahon, R. G. 1998, *ApJ*, 502, L99+
- Hu, E. M., Cowie, L. L., McMahon, R. G., Capak, P., Iwamuro, F., Kneib, J., Maihara, T., & Motohara, K. 2002, *ApJ*, 568, L75
- Inoue, A. K. 2001, *AJ*, 122, 1788
- Iwata, I., et al. 2009, *ApJ*, 692, 1287
- Iye, M., et al. 2006, *Nature*, 443, 186
- Kashikawa, N., et al. 2006, *ApJ*, 648, 7
- Kennicutt, Jr., R. C. 1998, *ARA&A*, 36, 189
- Kornei, K. A., Shapley, A. E., Erb, D. K., Steidel, C. C., Reddy, N. A., Pettini, M., & Bogosavljević, M. 2010, *ApJ*, 711, 693
- Krueger, H., Fritze-v. Alvensleben, U., & Loose, H. 1995, *A&A*, 303, 41
- Labbé, I., et al. 2010, *ApJ*, 708, L26
- Lai, K., Huang, J., Fazio, G., Cowie, L. L., Hu, E. M., & Kakazu, Y. 2007, *ApJ*, 655, 704
- Lai, K., et al. 2008, *ApJ*, 674, 70
- Lawrence, A., et al. 2007, *MNRAS*, 379, 1599
- Madau, P. 1995, *ApJ*, 441, 18
- Malhotra, S., & Rhoads, J. E. 2004, *ApJ*, 617, L5
- Maraston, C. 2005, *MNRAS*, 362, 799
- Miyazaki, S., et al. 2002, *PASJ*, 54, 833
- Murayama, T., et al. 2007, *ApJS*, 172, 523
- Nilsson, K. K., Tapken, C., Møller, P., Freudling, W., Fynbo, J. P. U., Meisenheimer, K., Laursen, P., & Östlin, G. 2009, *A&A*, 498, 13
- Nilsson, K. K., et al. 2007, *A&A*, 471, 71
- Oesch, P. A., et al. 2010, *ApJ*, 709, L16
- Oke, J. B., & Gunn, J. E. 1983, *ApJ*, 266, 713
- Ono, Y., et al. 2010, *MNRAS*, 402, 1580
- Osterbrock, D. E., & Ferland, G. J. 2006, *Astrophysics of gaseous nebulae and active galactic nuclei*, ed. Osterbrock, D. E. & Ferland, G. J.
- Ouchi, M., et al. 2003, *ApJ*, 582, 60
- . 2008, *ApJS*, 176, 301
- . 2009a, *ApJ*, 696, 1164
- . 2009b, *ApJ*, 706, 1136
- . 2010, *ArXiv e-prints* (arXiv:1007.2961)
- Pascarelle, S. M., Windhorst, R. A., Keel, W. C., & Odewahn, S. C. 1996, *Nature*, 383, 45
- Pentericci, L., Grazian, A., Fontana, A., Salimbeni, S., Santini, P., de Santis, C., Gallozzi, S., & Giallongo, E. 2007, *A&A*, 471, 433
- Pirzkal, N., Malhotra, S., Rhoads, J. E., & Xu, C. 2007, *ApJ*, 667, 49
- Raiter, A., Fosbury, R. A. E., & Teimoorinia, H. 2010, *A&A*, 510, A109+
- Razoumov, A. O., & Sommer-Larsen, J. 2010, *ApJ*, 710, 1239
- Rhoads, J. E., Malhotra, S., Dey, A., Stern, D., Spinrad, H., & Jannuzi, B. T. 2000, *ApJ*, 545, L85
- Salpeter, E. E. 1955, *ApJ*, 121, 161
- Schaerer, D., & de Barros, S. 2009, *A&A*, 502, 423
- . 2010, *A&A*, 515, A73+
- Schaerer, D., & Vacca, W. D. 1998, *ApJ*, 497, 618

- Shapley, A. E., Steidel, C. C., Pettini, M., & Adelberger, K. L. 2003, *ApJ*, 588, 65
- Shapley, A. E., Steidel, C. C., Pettini, M., Adelberger, K. L., & Erb, D. K. 2006, *ApJ*, 651, 688
- Shimasaku, K., et al. 2006, *PASJ*, 58, 313
- Shioya, Y., et al. 2009, *ApJ*, 696, 546
- Stark, D. P., Ellis, R. S., Bunker, A., Bundy, K., Targett, T., Benson, A., & Lacy, M. 2009, *ApJ*, 697, 1493
- Stark, D. P., Ellis, R. S., Chiu, K., Ouchi, M., & Bunker, A. 2010, *ArXiv e-prints* (arXiv:1003.5244)
- Steidel, C. C., Giavalisco, M., Pettini, M., Dickinson, M., & Adelberger, K. L. 1996, *ApJ*, 462, L17+
- Steidel, C. C., Pettini, M., & Adelberger, K. L. 2001, *ApJ*, 546, 665
- Storey, P. J., & Hummer, D. G. 1995, *MNRAS*, 272, 41
- Taniguchi, Y., et al. 2005, *PASJ*, 57, 165
- Tokunaga, A. T., Simons, D. A., & Vacca, W. D. 2002, *PASP*, 114, 180
- Vanzella, E., et al. 2009, *ApJ*, 695, 1163
- Warren, S. J., et al. 2007, *MNRAS*, 375, 213
- Wise, J. H., & Cen, R. 2009, *ApJ*, 693, 984
- Yajima, H., Choi, J., & Nagamine, K. 2010, *ArXiv e-prints* (arXiv:1002.3346)
- Zackrisson, E., Bergvall, N., & Leitert, E. 2008, *ApJ*, 676, L9